Volume 4
Number 8
August 2024
Pages 833–960

Environmental Science
Atmospheres

rsc.li/esatmospheres

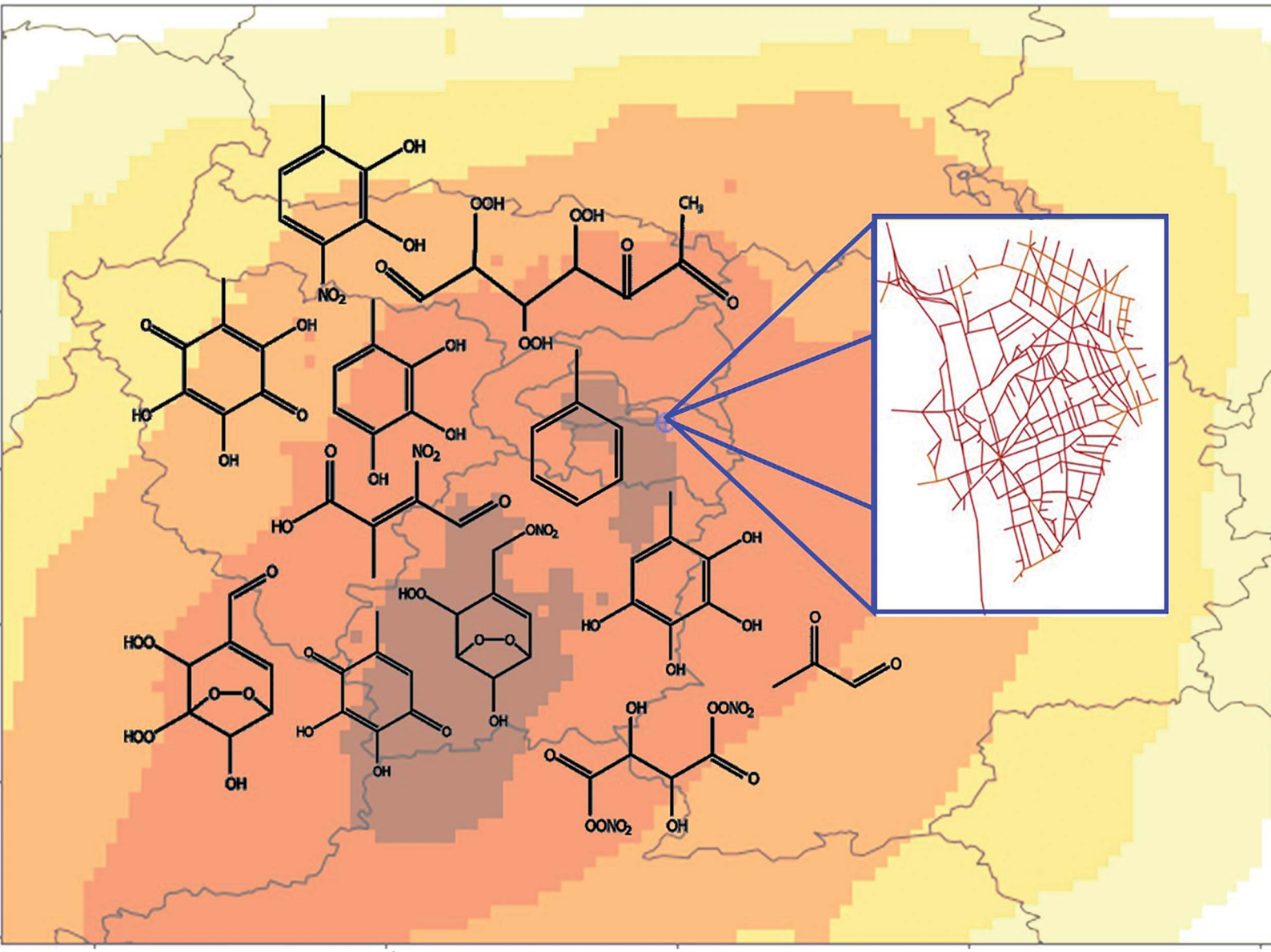

ISSN 2634-3606

ROYAL SOCIETY OF CHEMISTRY

PAPER
Karine Sartelet *et al.*
Modelling molecular composition of SOA from toluene photo-oxidation at urban and street scales

Environmental Science: Atmospheres

ROYAL SOCIETY OF CHEMISTRY

PAPER

View Article Online
View Journal | View Issue

Cite this: *Environ. Sci.: Atmos.*, 2024, **4**, 839

Modelling molecular composition of SOA from toluene photo-oxidation at urban and street scales†

Karine Sartelet, *[a] Zhizhao Wang, ‡[ab] Victor Lannuque,[a] Siddharth Iyer, [c] Florian Couvidat[b] and Thibaud Sarica§[a]

Near-explicit chemical mechanisms representing toluene SOA formation are reduced using the GENOA algorithm and used in 3D simulations of air quality over Greater Paris and in the streets of a district near Paris. The SOA concentrations formed by the toluene photo-oxidation are found to mostly originate from molecular rearrangement with ring opening of a bicyclic peroxy radical (BPR) with an O–O bridge (45%), followed by OH-addition on the aromatic ring (22%), Highly Oxygenated organic Molecules (HOM) formation without ring opening (13%), condensation of methylnitrocatechol (8%), irreversible formation of SOA from methylglyoxal (6%), and ring-opening pathway (3%). The concentrations simulated using the most comprehensive reduced chemical scheme (rdc. Mech. 3) are also compared to those simulated with a SOA scheme based on chamber measurements, and one reduced from the Master Chemical Mechanism. Using rdc. Mech 3 leads to between 50% and 75% more toluene SOA concentrations than the other schemes, mostly because of molecular rearrangement. The SOA compounds from rdc. Mech. 3 are more oxidized and less volatile, with molecules of different functional groups. Concentrations of methylbenzoquinones, which may be of particular health interest, represent about 0.5% of the toluene SOA concentrations. Those are slightly higher in streets than in the urban background (by 2%).

Received 19th April 2024
Accepted 14th June 2024

DOI: 10.1039/d4ea00049h

rsc.li/esatmospheres

Environmental significance

Toluene is one of the major monocyclic aromatic precursors of secondary organic aerosol (SOA) formation. Most SOA models used in 3D modelling oversimplify the chemical pathways leading to SOA formation and therefore may not accurately describe SOA formation under all environmental conditions. Here, near-explicit mechanisms of toluene SOA formation are reduced using the GENOA algorithm, preserving molecules and key chemical pathways. A recently highlighted pathway (molecular rearrangement of *ipso*-bicyclic peroxy radicals) is also added and found to be the main pathway for toluene SOA formation. This 3D molecular description of SOA, combined with multi-scale modelling, makes it possible to map the concentration and properties of pollutants of health concern from the regional scale down to the street level.

1 Introduction

High concentrations of organic aerosols are observed over cities,[1] with a strong contribution of solid-fuel combustion and traffic.[2] They are difficult to model, because of difficulties to estimate emission factors for the different sources,[3–5] to identify the precursors[6] and to represent the transformation of the precursors into secondary organic aerosols (SOAs).[7] Regional-scale chemistry transport models are usually used to represent background urban concentrations.[8] However, they need to be coupled to a local-scale street network model[6] to be able to represent the concentrations in streets, which are often higher than the background ones for compounds associated with high traffic emissions such as nitrogen oxides (NO_2), black carbon (BC), and particulate matter (PM).[9,10]

Aromatics are anthropogenic compounds that have long been considered important for the formation of SOAs in cities[11] and toluene is often considered as one of the most important monocyclic aromatic precursors for SOA formation.[12] Moreover, toluene SOA might have a large health impact through the formation of quinones[13] and Reactive Oxygen Species (ROSs).[14]

Most SOA models used in 3D modelling are based on chamber experiments, employing approaches such as the two-

[a]CEREA, École des Ponts ParisTech, EDF R&D, IPSL, Marne la Vallée, France. E-mail: karine.sartelet@enpc.fr

[b]National Institute for Industrial Environment and Risks (INERIS), 60550 Verneuil-en-Halatte, France

[c]Aerosol Physics Laboratory, Tampere University, FI-33101 Tampere, Finland

† Electronic supplementary information (ESI) available. See DOI: https://doi.org/10.1039/d4ea00049h

‡ Present address: University of California, Riverside, CA, USA, and National Center for Atmospheric Research, CO, USA.

§ Present address: Department of Civil and Environmental Engineering, Northeastern University, Boston, MA, USA.

compound Odum approach,[15] the surrogate approach,[16] and the volatility basis set.[17] Those models simplify the chemical pathways leading to SOA formation, and they use only a few aerosol model compounds to represent the myriad of formed oxidation products. Consequently, these simplified SOA schemes may not accurately describe the formation of SOA under all environmental conditions, especially at urban or street scales, where fast reactions such as autoxidation may be significant.[18]

More complex explicit or near-explicit chemical schemes exist, such as the Master Chemical Mechanism (MCM),[19] the SAPRC mechanism generation system,[20] and the Generator for Explicit Chemistry and Kinetics of Organics in the Atmosphere (GECKO-A).[21] These schemes are of great interest for SOA formation because they account for the various chemical pathways and environmental variations. However, they may not easily be used in 3D modelling due to computational resources limitations.[22] Furthermore, they account for the great variety of molecules and their different functional groups, which may be of particular interest to better understand the impact of SOA on human health. For example, the decomposition of organic hydroperoxides,[23,24] peracids,[25] and carbonyls[26] can lead to the formation of ROS.[27] Toluene SOA may also affect ROS formation *via* the redox cycling of quinoid compounds.[14,27] As these explicit or near-explicit chemical schemes are too computationally expensive to be used in 3D air-quality models, some studies have developed reduced mechanisms from them.[28–30] Cao and Jang[31] developed a reduced mechanism for toluene from MCM. Wang *et al.*[32,33] developed the GENerator of reduced Organic Aerosol mechanism (GENOA) algorithm that can automatically reduce detailed chemical mechanisms regarding SOA formation under various atmospheric conditions.

Many laboratory studies have investigated the oxidation mechanism of toluene to understand the different chemical pathways leading to SOA formation.[34–40] Lannuque *et al.*[39] built a detailed mechanism for toluene oxidation based on MCM and GECKO-A, which follows recent literature to improve cresol formation,[41] accounts for ring-scission chemistry[34] and the formation of Highly Oxygenated Molecules (HOMs) by autoxidation.[35] However, this mechanism did not consider the molecular rearrangement of bicyclic peroxy radicals (BPRs), which was recently pointed out as a potential key pathway to form SOAs.[40] In order to investigate the influence of different chemical pathways on SOA formation, GENOA is used here to generate condensed toluene SOA mechanisms from MCM and from Lannuque *et al.*[39] These reduced chemical mechanisms are implemented in the aerosol model SSH-aerosol,[42] coupled to the 3D regional and street air-quality models Polair3D[43] and MUNICH.[44] After a description of the toluene mechanisms and their reduction, the influence of the reduced chemical mechanisms on toluene SOA concentrations and composition at urban and street scales is investigated in this study.

2 Toluene mechanisms

2.1 Description

Following the MCM v3.3.1, the oxidation of toluene leads to several pathways: (i) the addition of an OH function on the aromatic ring, forming BPR with an O–O bridge (65%), (ii) the addition of an OH function on the ring forming cresol (18%), (iii) the addition of an OH function on the ring forming an epoxide with ring opening (10%), and (iv) the hydrogen abstraction from the methyl group (7%).

In Lannuque *et al.*,[39] the toluene oxidation mechanism was modified by using GECKO-A to generate the oxidation mechanism for non-aromatic compounds, thereby improving the representation of methylglyoxal, a major gaseous compound formed during the toluene oxidation. Additionally, a formation pathway of HOMs from the BPRs was incorporated following Wang *et al.*[35] Furthermore, in the cresol formation pathway, the successive addition of an alcohol function on the aromatic ring was included following Schwantes *et al.*[41] New reaction pathways for ring-opening chemistry or formation of furan-like compounds were also added following Jang and Kamens.[34]

Although the formation of a BPR by an attack of OH on the aromatic ring in the *ortho*-position is favored,[45–47] Iyer *et al.*[40] has shown that ring attack in the *ipso*-position could also lead to the formation of SOA by molecular rearrangement of the *ipso*-BPR, accounting for 7% of ring attack. Due to the addition of the *ipso*-BPR in the first oxidation step of toluene, the branching ratios of ring attack pathways are adjusted (multiplied by 0.93 to include the *ipso*-BPR branching ratio). Similarly to *ortho*-BPR in the Lannuque *et al.*[39] mechanism, *ipso*-BPR is considered to undergo oxidation by NO, HO_2, RO_2, and NO_3 with the same kinetic rates as *ortho*-BPR. Concerning the molecular rearrangement, only the main pathway leading to SOA formation in Iyer *et al.*[40] is kept: *ipso*-BPR undergoes molecular rearrangement leading to a ring-broken RO_2 (P-C_2), which then undergoes a 1,6 H-shift and an O_2 addition, forming the peroxy radical R1b-RO_2. R1b-RO_2 isomerizes *via* a 1,6 H-shift at a rapid rate of 200 s^{-1}, quickly followed by O_2 addition to form O_9-RO_2 $C_7H_9O_9$. Both of these reactions occur too fast for bimolecular reactions (with HO_2/NO) to play a significant role. The $C_7H_9O_9$ could continue to undergo rapid unimolecular reactions to form higher oxidized RO_2s. However, accurate rates for this molecule are not available, and because $C_7H_9O_9$ is modelled to be predominantly in the condensed phase in the atmosphere, further reactions are not included. The saturation vapor pressure of condensable compounds is estimated using UManSysProp,[48] with the method of Myrdal and Yalkowsky[49] for vapor pressure and the method of Nannoolal *et al.*[50] for the boiling point.

Finally, three near-explicit mechanisms for toluene gaseous oxidation are considered:

- The "Mech. 1" is the mechanism available in MCM v3.3.1.[51,52]
- The "Mech. 2" corresponds to the mechanism described in Lannuque *et al.*[39] Based on the MCM and GECKO-A[21] mechanisms updated for cresol, ring-scission chemistry, and the formation of HOM, it also represents the irreversible partitioning pathway for methylglyoxal.[53]
- The "Mech. 3" mechanism corresponds to the "Mech. 2" mechanism with the addition of the *ipso*-BPR pathway. It is considered the most comprehensive mechanism among the three in terms of pathways leading to SOA formation.

2.2 Reduced toluene SOA mechanisms

The GENOA v2.0 (ref. 33) algorithm is employed to reduce the near-explicit toluene chemical mechanisms regarding SOA formation. Within GENOA, reduction strategies are applied to search for reduction candidates, such as merging similar compounds, jumping over rapidly degrading radicals, and removing reactions or species with low contributions to SOA production. These reduction candidates are then evaluated using 0D simulations under a dataset of representative atmospheric conditions, with only those meeting selection criteria being incorporated into the reduced mechanism. This search-and-evaluate process continues until no further reductions are viable, and the final reduced SOA mechanism is eventually evaluated under a large dataset covering a wide range of conditions. As GENOA primarily aims to preserve SOA formation, its reduction evaluation is based on the total SOA concentration and composition simulated using the aerosol model SSH-aerosol,[42] accounting for different aerosol phenomena (*e.g.*, non-ideality and hydrophilic/hydrophobic partitioning).

The reduction of toluene SOA mechanisms (*i.e.*, Mech. 1 and Mech. 2) adopted a GENOA configuration similar to Wang *et al.*[33] Three datasets of atmospheric conditions are selected over Europe for reduction evaluation at different reduction stages. In the early stage of reduction, an eight-condition dataset is adopted, including six extreme conditions of Wang *et al.*[33] and two high-NOx Paris street conditions from Sarica *et al.*[6] Afterward, the evaluation dataset changes to a broader 152-condition dataset to better represent general atmospheric conditions. Finally, a comprehensive dataset of 9433 European conditions is used for the final evaluation of the reduced mechanism. Simulations are set for five days with different starting times (0 h, 7 h, and 20 h) to include SOA formation and aging in response to nighttime and daytime chemistry, potentially influenced by traffic rush hours.

The final reduced mechanisms of Mech. 1 and Mech. 2 are comparable in size and accuracy, as detailed in Table 1. The mechanisms reactions and main compounds are detailed in the ESI (Sections S1 and S2†). Maps of the relative error between the near-explicit and reduced mechanisms over the 9433 European conditions are displayed in Section S3 of the ESI.† As the addition of the *ipso*-BPR pathway leads to only one aerosol species, the reduced mechanism of Mech. 3 (rdc. Mech. 3) is obtained by simply adding the *ipso*-BPR pathway to the reduced mechanism of Mech. 2 (rdc. Mech. 2) and by modifying the other branching ratios, as described in Section 2.1.

For comparison with mechanisms commonly used in 3D simulations,[6] the highly simplified hydrophilic/hydrophobic organic (H^2O) SOA mechanism, is also adopted. The H^2O mechanism, which uses a surrogate approach based on chamber experiments,[42,54] models toluene SOAs with three surrogates: AnClP formed by reactions of toluene with OH and HO_2/RO_2 under low-NOx conditions, as well as AnBlP and AnBmP, formed by reactions of toluene with OH and NO/NO_3 under high-NOx conditions.

2.3 Reduced mechanism with quinone formation

According to Lannuque *et al.*,[39] Schwantes *et al.*,[41] methylbenzoquinone (MBQN) molecules are formed during the oxidation of methylcatechol (dihydroxytoluene), which itself is derived from cresol, followed by successive additions of alcohol functions on the aromatic ring. This oxidation pathway is kept in the rdc. Mech. 3, as it leads to the formation of TOL3OH (trihydroxytoluene) and TOL4OH (tetrahydroxytoluene), which are some of the main compounds of toluene SOAs (see Section 3.2). However, the formation of MBQN may not be necessary for reduced SOA mechanisms that aim to represent the total SOA mass, as its influence on SOA formation is low. Nevertheless, because of the potential significant health effects of these molecules,[13,27] the formation pathways of hydroxy methylbenzoquinone (MBQN1OH), dihydroxy methylbenzoquinone (MBQN2OH), trihydroxy methylbenzoquinone (MBQN3OH) are preserved in the rdc. Mech. 3 (see Section S1 of the ESI†).

2.4 Evaluation of the mechanisms

The SOA concentrations formed from toluene photo-oxidation in the flow tube experiment of Lannuque *et al.*[39] using the different toluene SOA mechanisms are compared in Fig. 1. Wall losses are modelled as in Lannuque *et al.*[39]. The measured SOA concentrations are 16 μg m^{-3}. They are well reproduced by the

Table 1 Mechanism**** size and accuracy (in terms of reduction errors in %,[33]) before (noted as "ref") and after (noted as "rdc") the GENOA v2.0 reduction process

Scheme	Reaction	Gas	Aerosol	Ave.err	Max.err
ref. Mech. 1	814	270	132	—	—
rdc. Mech. 1	48	28	10	3.1	71
ref. Mech. 2	494	210	105	—	—
rdc. Mech. 2	48	31	9	2.7	28
rdc. Mech. 3	54	35	10	—	—

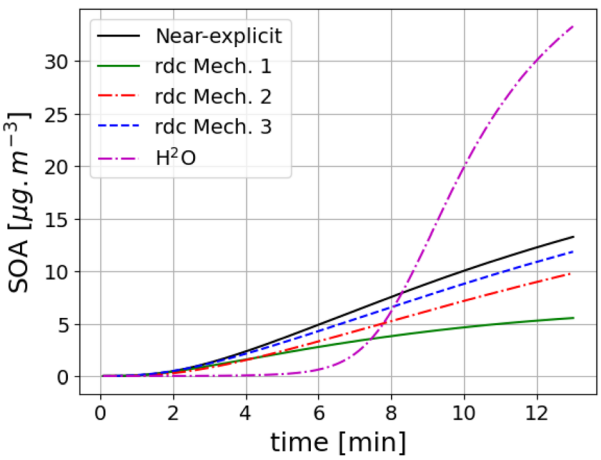

Fig. 1 Toluene SOA concentrations (in μg m^{-3}) simulated with different toluene SOA mechanisms (the near-explicit mechanism Mech. 2, the reduced mechanisms rdc. Mech. 1, rdc. Mech. 3 and H^2O) for the flow tube experiment of Lannuque *et al.*[39]

near-explicit scheme of Lannuque *et al.*[39] (Mech. 2) and the rdc. Mech. 3, with SOA concentrations of 13.3 μg m^{-3} and 11.9 μg m^{-3}, respectively. The concentrations simulated with rdc. Mech. 2 are about 16% lower than those of Mech. 3, indicating a limited impact of molecular rearrangement of the *ipso*-BPR pathway in this flow tube experiment. The SOA concentrations are very under-estimated using rdc. Mech. 1, with a SOA concentration of 5.6 μg m^{-3}, and they are over-estimated using H^2O, with a SOA concentration of 33.5 μg m^{-3}. Using H^2O leads to smaller SOA concentrations compared to other mechanisms at the beginning of the experiment, when the concentrations are low, and higher concentrations are the end.

3 3D simulations over Greater Paris down to the street scale

3.1 Model set-up

The simulations are conducted over two months, starting on the 1st of May 2014, using the modelling chain WRF-Polair3D/MUNICH/SSH-aerosol[6,55] to represent the evolution of concentrations at the regional scale (0.02 × 0.02 horizontal resolution) and the local scale (street network of an eastern suburb of Paris). The street network is displayed in Fig. 3. The streets are discretised into segments of uniform height and width. Concentrations are assumed to be homogeneous in each street segment. The background concentrations above the streets are those simulated with Polair3D. At intersections, pollutants may be transported from one street segment to another. The wind profile in streets and vertical/horizontal transfer coefficients were parameterized by adapting a flow parametrization for sparse vegetated canopy to street canyons using computational fluid dynamic simulations, as described in Maison *et al.*[56] The wind velocity in the streets is estimated using the friction velocity above the streets simulated with WRF, the wind angle with the street, and the street characteristics.[56] The exchange between the background and street concentrations depends on the gradient concentrations, the street characteristics and the meteorology.[44,56,57]

The model setup is detailed in Sarica *et al.*,[6] which also presents the model validation by comparisons to measurements of BC, NO_2, PM_{10}, $PM_{2.5}$, and organic matter over the year 2014. The model validation over the two months simulated here is presented in Section S4 of the ESI.† The SSH-aerosol model is used in the WRF-Polair3D/MUNICH chain to represent the gas-phase chemistry and aerosol dynamics. In Sarica *et al.*,[6] simulations were performed over Greater Paris using the H^2O mechanism, with boundary conditions from a simulation over France.[4] Here, sensitivity simulations are run over Greater Paris using alternatively the reduced mechanisms rdc. Mechs. 1 to 3 for the formation of toluene SOA. As the newly added toluene SOA compounds were not previously simulated over France, the boundary conditions for those compounds are set to 0.

3.2 Concentrations of toluene SOA

Fig. 2 and 3 show the concentrations of toluene and toluene SOA during this two-month period, simulated using the WRF-Polair3D/MUNICH/SSH-aerosol and the rdc. Mech. 3, which is the most comprehensive reduced chemical mechanism among those discussed in this work. The toluene concentrations are notably higher in the city of Paris, particularly in the center of the domain, and in streets with high traffic. Spatial heterogeneities are more significant for toluene than for toluene SOA. Average toluene SOA concentrations are elevated in the center of Paris and its nearby suburbs, in the main direction of the urban plume, as shown in Fig. 2. Concentrations of toluene SOA are quite homogeneous across different streets.

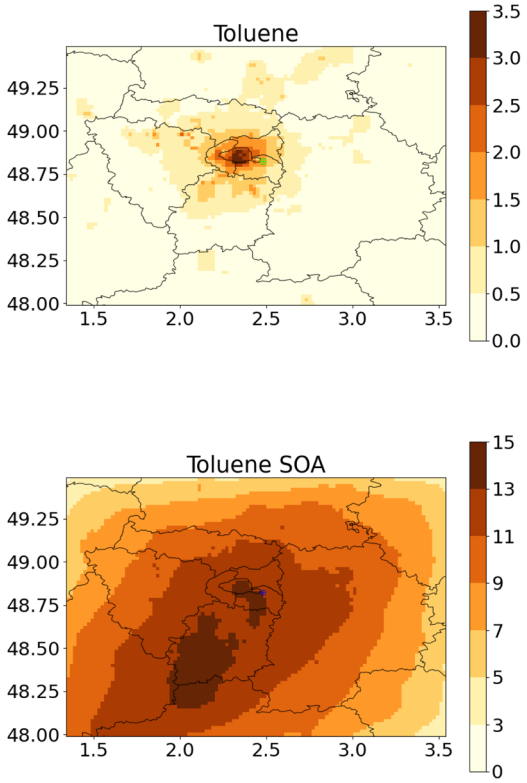

Fig. 2 Regional-scale toluene concentrations (left panel, in μg m^{-3}) and toluene SOA concentations (right panel, in ng m^{-3}) simulated with the rdc. Mech. 3, in May–June 2014.

To assess the impact of the representation of toluene SOA chemistry in 3D air-quality modelling, sensitivity simulations are conducted by changing the toluene SOA mechanism.

The more comprehensive rdc. Mech. 3 is replaced by other toluene SOA reduced mechanisms, including rdc. Mech. 1, rdc. Mech. 2, and the simpler H^2O mechanism. The differences between the mechanisms are different than those simulated in the flow tube, because favorable reactions pathways may differ depending on the reaction ratios of the precursor with the oxidants O_3, OH and NO_3, and on the reaction ratios of RO_2 species with NO, HO_2, NO_3, and other RO_2 species.[58] The toluene SOA concentrations are between 45% and 70% lower with the H^2O mechanism (Fig. 4), and between 50% and 70% lower with the rdc. Mech. 1 mechanism compared to rdc. Mech. 3. The concentration differences between rdc. Mech. 1 and rdc. Mech. 3 are generally uniform over the domain, whereas the differences between H^2O and rdc. Mech. 3 are slightly lower

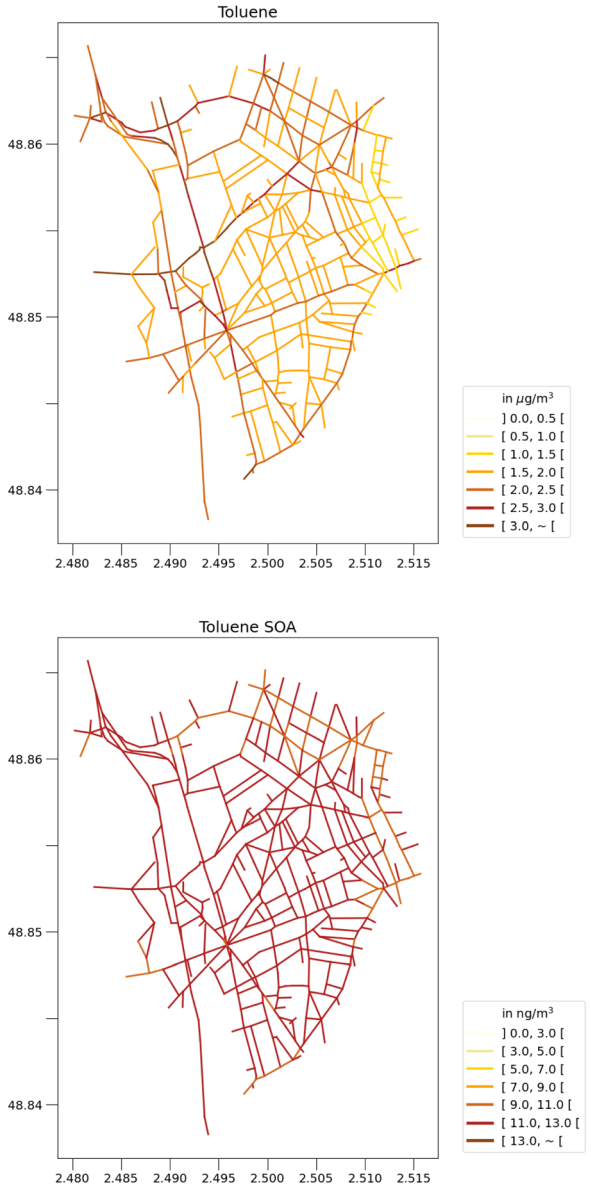

Fig. 3 Street-scale toluene concentrations (left panel, in µg m^{-3}) and toluene SOA concentations (right panel, in ng m^{-3}) simulated with the rdc. Mech. 3, in May–June 2014.

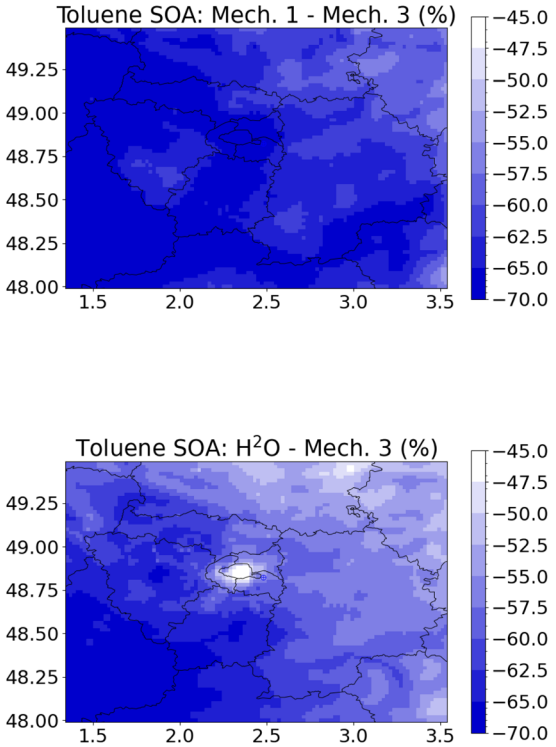

Fig. 4 Relative differences (%) of toluene SOA concentrations in May–June 2014 between rdc. Mech. 1 and rdc. Mech. 3 (left panel) and between H^2O and rdc. Mech. 3 (right panel).

over Paris city. The higher concentrations simulated with rdc. Mech. 3 are mostly due to SOA formed from the molecular rearrangement of the BPR radical, which represents 45% of the toluene SOA concentrations in rdc. Mech. 3. The concentrations of SOA from the molecular rearrangement of *ipso*-BPR are particularly high over Paris, where toluene concentrations are the highest and within the city plume (see Section S5 of the ESI†). Indeed, with rdc. Mech. 2 where *ipso*-BPR SOA is not taken into account, the differences between the mechanisms are lower, ranging from −13% to −38% for rdc. Mech. 1 compared to rdc. Mech. 2 and from 18% and −42% for H^2O compared to rdc. Mech. 2. Over Paris city, the concentrations simulated using H^2O are higher than those simulated with rdc. Mech. 2. These results highlight the significant influence of molecular rearrangement of *ipso*-BPR on toluene SOA concentrations, regardless of the environmental conditions.

The highest concentrations simulated with rdc. Mech. 3 are not only due to *ipso*-BPR SOA, but also to several toluene SOA formation pathways added by Lannuque *et al.*[39] The most influential pathway is the OH addition to the aromatic cycle, which is particularly efficient at forming SOA in the city plume. Further analysis of the main molecular compounds in rdc. Mech. 3 is provided in the next section.

At the street scale, the toluene SOA concentrations are similar to those above the streets, *i.e.* in the city's urban background. The differences in toluene SOA concentrations between the mechanisms are also very similar to those observed at the regional scale, but slightly stronger. The differences between the toluene SOA concentrations simulated with rdc. Mech. 1 and rdc. Mech. 3 range from −86% and −88% in the streets, whereas they are −67% above the street network in the urban background. The differences between the toluene SOA concentrations simulated with H^2O and rdc. Mech. 3 range from −56% and −38% in the streets, whereas they are about −53% above the street network. These higher differences between the mechanisms are linked to differences in the volatility of the compounds between the mechanisms. The volatility of the compounds of rdc. Mech. 1 and H^2O is much higher than that of rdc. Mech. 3: on average, the particle phase toluene SOA concentrations represent 95% of the gas and particle phase SOA concentrations in rdc. Mech. 3, whereas they account for only 41% and 21% in rdc. Mech. 1 and H^2O, respectively.

The model accounts for the exchange/transport between the urban background and the street concentrations. Particles may not only be emitted or formed in the streets, they may be transported from the background to the street. During this transport, the particle-phase compounds of high volatility that are not significantly produced in the street (and are formed at a larger scale) tends to shift to the gas phase due to the dilution of the background concentrations within the street volume. However, the street and background concentrations are very similar in rdc. Mech. 3, mainly because most toluene SOA compounds are highly oxidized and have low volatility, as discussed in the subsequent section.

3.3 Composition of toluene SOA

3.3.1 Regional-scale urban background. Although the different toluene mechanisms lead to moderate differences in terms of toluene SOA concentrations (less than 70% differences), the molecular composition differs significantly. The daily composition of toluene SOA remains relatively stable during the two months of simulation (Fig. 5). In rdc. Mech. 1, the main products are formed from the oxidation of methylcatechol in the cresol chemical pathway: MNCATECH represents 59% of the toluene SOA simulated with rdc. Mech. 1, *i.e.* $\simeq$1.9 ng m^{-3}, and MNNCATCOOH represents 10%, *i.e.* $\simeq$0.3 ng m^{-3}. In contrast, the equivalents in rdc. Mech. 3 (MNCATECH and HOM2ONO2) contribute significantly less to the toluene SOA, about 8.5% and 5%, respectively, corresponding to 0.8 ng m^{-3} and 0.4 ng m^{-3}. The second most formed product in rdc. Mech. 1 is TLFUOOH, constituting 18% of the toluene SOA or 0.6 ng m^{-3}. However, this compound was not retained individually and was merged with other compounds during the reduction of Mech. 2, because of its relatively low contribution to SOA formation. The predominant role of methylcatechol oxidation products in MCM and, by extension, in rdc. Mech. 1, was pointed out in several studies as being excessively high.[36,39]

In rdc. Mech. 3, the main products correspond to the molecular rearrangement of *ipso*-BPR with ring opening ($C_7H_9O_9$ at 45%, 4.5 ng m^{-3}), followed by the products formed by the successive addition of the alcohol function –OH to the aromatic ring (TOL3OH at 15%, 1.5 ng m^{-3}, and TOL4OH at 6%, 0.6 ng m^{-3}), and by the HOM formation pathway from the *ortho*-BPR without ring opening (HOM2O, 9%, 0.9 ng m^{-3}, and HOM2ONO2, 4%, 0.4 ng m^{-3}). The formation of methylnitrocatechol contributes to about 8%, and the irreversible pathway of methylglyoxal (IRMGLY) to about 6%, 0.6 ng m^{-3}. The ring-opening pathway (PP4000) has a low but non-negligible contribution (about 3%, 0.3 ng m^{-3}).

The toluene SOA molecules significantly differ between rdc. Mech. 1 and rdc. Mech. 3, leading to distinct contributions of the functional groups constituting these molecules, as illustrated in Fig. 6. This figure compares the functional groups in the toluene SOA of rdc. Mech. 1 and rdc. Mech. 3 across the simulation domain and period. The concentrations associated with each functional group are estimated by multiplying the concentrations of each molecule by the molar mass ratio between the functional group and the molecule. In rdc. Mech. 1, the alkyl –C (22%), alcohol –OH (24%) and nitroaromatic -ACNO2 (20%) groups are dominant, while in rdc. Mech. 3 the hydroperoxyl group –CO–OH (29%), the carbonyl group –RCO (20%) and alcohol –OH (19%) are very high. The concentrations linked to the nitroaromatic group are higher in rdc. Mech. 1 than in rdc. Mech. 3. Although the nitroaromatics could be genotoxics,[59] the high methylnitrocatechol simulated in rdc. Mech. 1 may not be realistic.[36] Furthermore, dinitro-aromatics could be much more toxic than mononitro-aromatics,[59] and the only dinitro-aromatic simulated is dinitro-cresol, which represents 0.12% of the toluene SOA concentrations in rdc. Mech. 1, and 0.04% of the toluene SOA concentrations in rdc. Mech. 3. Considering the toxicity of

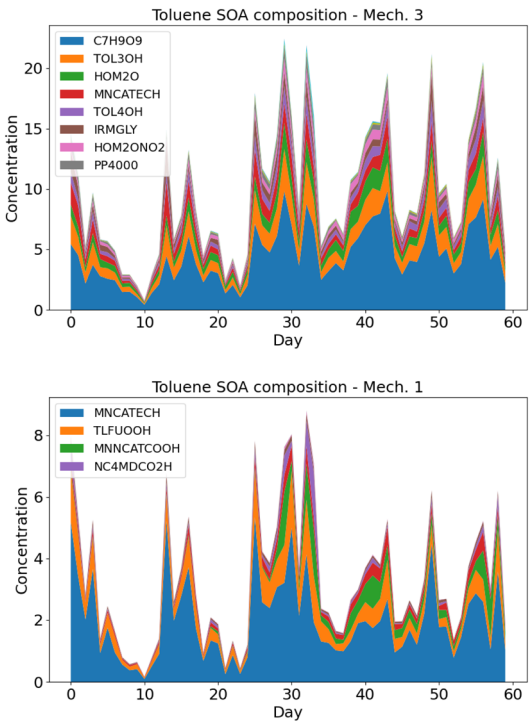

Fig. 5 Average toluene SOA composition over Greater Paris in May–June 2014, using rdc. Mech. 3 (left panel) and rdc. Mech. 1 (right panel).

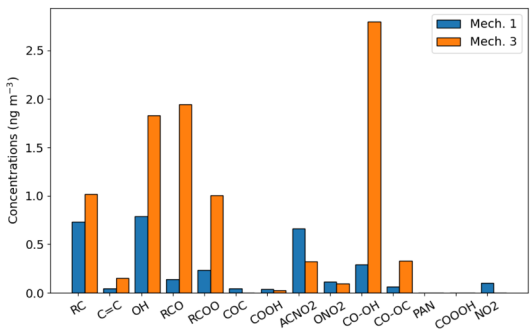

Fig. 6 Functional groups simulated in the average toluene SOA concentrations over Greater Paris in May–June 2014, using rdc. Mech. 1 and rdc. Mech 3: alkyl (RC), double C bound (C=c), alcohol (OH), carbonyl (RCO), esther (RCOO), ether (COC), acid (COOH), nitroaromatic (ACNO2), nitrate (ONO2), hydroperoxide (CO–OH), peroxide (CO–OC), peroxyacyl nitrates (PAN), peroxyacetyl acid (COOOH), nitroalkyl (NO2).

Table 2 Comparison of total toluene SOA composition simulated with rdc. Mech. 3 above the street network and in the streets over May–June 2014 (in ng m^{-3})

- *ipso*-BPR molecular rearrangement w. ring opening ($C_7H_9O_9$)	6.2	6.1	1.00
- OH-addition from MCATECH (TOL3OH, TOL4OH, TOL3OH1NO2)	3.0	3.0	1.00
- Methylnitrocathecol and oxidation products (MNCATECH, NC4MDCO2H)	1.9	1.9	1.00
- BPR HOM formation without ring opening (HOM2O)	1.1	1.1	1.01
- Irreversible formation of SOA from methylglyoxal (IRMGLY)	0.9	0.9	1.01
- Ring-opening pathway (PP4000)	0.5	0.5	1.00
- HOM2ONO2	0.5	0.5	1.00
- Formation of MBQN (MBQN1OH, MBQN2OH, MBQN3OH)	0.2	0.2	1.02

hydroperoxide and carbonyls due to their influences on oxidative potential,[23,26] the functional group distribution of the various compounds suggests notable health impacts of the compounds simulated with rdc. Mech. 3.

For health impacts, the concentrations of quinones may also specifically matter. The concentrations of MBQN are only simulated in rdc. Mech. 3. They constitute a small fraction of toluene SOA: they represent on average 0.5% of the toluene SOA concentrations, distributed between MBQN2OH for 44% and MBQN3OH for 56%.

3.3.2 Street scale. The toluene SOA compositions simulated with rdc. Mech. 3 are similar at the street and regional scales. To understand if toluene SOAs are formed in the gas phase in the streets, Table 2 compares the total (gas and particle phases) concentrations averaged over the street network and those above it (background). A ratio of concentration between the background and the street concentrations close to 1 suggests that the compound is mainly formed at the regional scale, while a ratio above 1 indicates formation in the street. For most compounds, the ratio is close to 1 or only slightly higher, indicating that the formation in streets is low. Compounds with the highest street-to-background ratio include MBQN (1.02), HOM formation without ring opening (1.01), and irreversible formation of SOA from methylglyoxal (1.01), suggesting a slight formation of those compounds in the streets, allowing to represent the molecular composition of toluene SOA over Greater Paris and down to the streets of a district in the eastern part.

4 Conclusions

Near-explicit chemical mechanisms of toluene photo-oxidation were reduced using the GENOA algorithm to simulate SOA formation, preserving the main chemical pathways and molecules. Three reduced mechanisms were considered: one derived from the Master Chemical Mechanism (rdc. Mech 1.), one derived from Lannuque *et al.*[39] (rdc. Mech. 2). The third adds a recently highlighted pathway (molecular rearrangement of *ipso*-bicyclic peroxy radicals) to the mechanism reduced from Lannuque *et al.*[39] (rdc. Mech. 3). These SOA mechanisms are implemented in the multi-scale modelling chain Polair3D/MUNICH/SSH-aerosol The more comprehensive rdc. Mech. 3 is replaced by other toluene SOA reduced mechanisms, including rdc. Mech. 1, rdc. Mech. 2, and the simpler H^2O mechanism built from chamber measurements. The toluene SOA concentrations are between 45% and 70% lower with the different mechanism compared to rdc. Mech. 3., because of the molecular rearrangement of the *ipso*-BPR radical, which represents 45% of the toluene SOA concentrations in rdc. Mech. 3.

The toluene SOA molecules differ significantly between rdc. Mech. 1 and rdc. Mech. 3. In rdc. Mech. 1, the main products are formed from the oxidation of methylcatechol in the cresol chemical pathway (69% of toluene SOA), whereas in rdc. Mech. 1, the main products are formed from the molecular rearrangement of *ipso*-bicyclic peroxy radicals (45%) and by the successive addition of the alcohol function –OH to the aromatic ring (21%). This leads to distinct contributions of the functional groups constituting the SOA molecules in the different mechanisms. In rdc. Mech. 1, the alkyl –C (22%), alcohol –OH (24%) and nitro-aromatic –ACNO2 (20%) groups are dominant, whereas in rdc. Mech. 3 the hydroperoxyl group –CO–OH (29%), the carbonyl group –RCO (20%) and alcohol –OH (19%) are very important.

In future work, the methodology presented here should be generalised to other SOA precursors. It will allow a more accurate description of the molecular composition of SOA in cities, taking into account the different oxidation pathways. This will allow better estimation of changes in concentrations in relation to changes in emissions,[29] but also strengthen the links between organic aerosol concentrations and health effects.

Data availability

Data for regional-scale model evaluation are publicly available from **https://www.geodair.fr/**. The code for the H_2O chemical mechanism is available at **https://github.com/sshaerosol/ssh-aerosol**. The new chemical schemes supporting this article are described in the ESI.†

Author contributions

KS: conceptualization, formal analysis, investigation, methodology, software, resources, validation, vizualisation, writing – original draft ZW: formal analysis, investigation, methodology, software, validation, vizualisation, writing – review & editing; VL: software, methodology, writing – review & editing; SI: methodology, writing – review & editing; FC: software, writing – review & editing; TS: validation, writing – review & editing.

Conflicts of interest

There are no conflicts to declare.

Acknowledgements

This work was partially funded by DIM QI2 (Air Quality Research Network on air quality in the Île-de-France region), POLEMICS project of the Agence Nationale de la Recherche (ANR) program (grant ANR-18-CE22-0011), and the European Union's Horizon 2020 Research and Innovation Programme (RI-URBANS (grant no. 101036245)).

Notes and references

1 R. M. Harrison, *Philos. Trans. R. Soc., A*, 2020, **378**, 20190319.
2 G. Chen, F. Canonaco, A. Tobler, W. Aas, A. Alastuey, J. Allan, S. Atabakhsh, M. Aurela, U. Baltensperger, A. Bougiatioti, J. F. De Brito, D. Ceburnis, B. Chazeau, H. Chebaicheb, K. R. Daellenbach, M. Ehn, I. El Haddad, K. Eleftheriadis, O. Favez, H. Flentje, A. Font, K. Fossum, E. Freney, M. Gini, D. C. Green, L. Heikkinen, H. Herrmann, A.-C. Kalogridis, H. Keernik, R. Lhotka, C. Lin, C. Lunder, M. Maasikmets, M. I. Manousakas, N. Marchand, C. Marin, L. Marmureanu, N. Mihalopoulos, G. Močnik, J. Necki, C. O'Dowd, J. Ovadnevaite, T. Peter, J.-E. Petit, M. Pikridas, S. Matthew Platt, P. Pokorná', L. Poulain, M. Priestman, V. Riffault, M. Rinaldi, K. Rózański, J. Schwarz, J. Sciare, L. Simon, A. Skiba, J. G. Slowik, Y. Sosedova, I. Stavroulas, K. Styszko, E. Teinemaa, H. Timonen, A. Tremper, J. Vasilescu, M. Via, P. Vodička, A. Wiedensohler, O. Zografou, M. Cruz Minguillón and A. S. Prévôt, *Environ. Int.*, 2022, **166**, 107325.
3 B. C. McDonald, J. A. de Gouw, J. B. Gilman, S. H. Jathar, A. Akherati, C. D. Cappa, J. L. Jimenez, J. Lee-Taylor, P. L. Hayes, S. A. McKeen, Y. Y. Cui, S.-W. Kim, D. R. Gentner, G. Isaacman-VanWertz, A. H. Goldstein, R. A. Harley, G. J. Frost, J. M. Roberts, T. B. Ryerson and M. Trainer, *Science*, 2018, **359**, 760–764.
4 K. Sartelet, S. Zhu, S. Moukhtar, M. André, J. André, V. Gros, O. Favez, A. Brasseur and M. Redaelli, *Atmos. Environ.*, 2018, **180**, 126–137.
5 A. Maison, L. Lugon, S.-J. Park, A. Baudic, C. Cantrell, F. Couvidat, B. D'Anna, C. Di Biagio, A. Gratien, V. Gros, C. Kalalian, J. Kammer, V. Michoud, J.-E. Petit, M. Shahin, L. Simon, M. Valari, J. Vigneron, A. Tuzet and K. Sartelet, *EGUsphere*, 2023, **2023**, 1–57.
6 T. Sarica, K. Sartelet, Y. Roustan, Y. Kim, L. Lugon, B. Marques, B. D'Anna, C. Chaillou and C. Larrie, *Environ. Pollut.*, 2023, **332**, 121955.
7 Y. Kim, F. Couvidat, K. Sartelet and C. Seigneur, *J. Air Waste Manage. Assoc.*, 2011, **61**, 1218–1226.
8 K. Sartelet, Y. Kim, F. Couvidat, M. Merkel, T. Petäjä, T. Sciare and A. Wiedensohler, *Atmos. Chem. Phys.*, 2022, **22**, 8579–8596.
9 L. Lugon, K. Sartelet, Y. Kim, J. Vigneron and O. Chrétien, *Atmos. Chem. Phys.*, 2020, **20**, 7717–7740.
10 L. Lugon, Y. Kim, J. Vigneron, O. Chrétien, M. André, J.-M. André, S. Moukhtar, M. Redaelli and K. Sartelet, *Atmos. Pollut. Res.*, 2022, **13**, 101365.
11 J. Peng, M. Hu, Z. Du, Y. Wang, J. Zheng, W. Zhang, Y. Yang, Y. Qin, R. Zheng, Y. Xiao, Y. Wu, S. Lu, Z. Wu, S. Guo, H. Mao and S. Shuai, *Atmos. Chem. Phys.*, 2017, **17**, 10743–10752.
12 D. Srivastava, T. Vu, S. Tong, Z. Shi and R. M. Harrison, *npj Clim. Atmos. Sci.*, 2022, **5**, 22.
13 T. Monks, R. Hanzlik, G. Cohen, D. Ross and D. Graham, *Toxicol. Appl. Pharmacol.*, 1992, **112**(1), 2–16.
14 Y. Wang, H. Kim and S. E. Paulson, *Atmos. Environ.*, 2011, **45**, 3149–3156.
15 J. R. Odum, T. Hoffmann, F. Bowman, D. Collins, R. C. Flagan and J. H. Seinfeld, *Environ. Sci. Technol.*, 1996, **30**, 2580–2585.
16 B. K. Pun, C. Seigneur and K. Lohman, *Environ. Sci. Technol.*, 2006, **40**, 4722–4731.
17 N. M. Donahue, A. L. Robinson, C. O. Stanier and S. N. Pandis, *Environ. Sci. Technol.*, 2006, **40**, 2635–2643.
18 Y. Wang, C. Flageul, A. Maison, B. Carissimo and K. Sartelet, *Environ. Pollut.*, 2023, **323**, 121210.
19 M. E. Jenkin, S. M. Saunders and M. J. Pilling, *Atmos. Environ.*, 1997, **31**, 81–104.
20 W. P. L. Carter, J. Jiang, J. J. Orlando and K. C. Barsanti, *EGUsphere*, 2023, **2023**, 1–65.
21 B. Aumont, S. Szopa and S. Madronich, *Atmos. Chem. Phys.*, 2005, **5**, 2497–2517.
22 J. Li, M. Cleveland, L. D. Ziemba, R. J. Griffin, K. C. Barsanti, J. F. Pankow and Q. Ying, *Atmos. Environ.*, 2015, **102**, 52–61.
23 H. Tong, A. Arangio, P. Lakey, T. Berkemeier, F. Liu, C. Kampf, W. Brune, U. Poschl and M. Shiraiwa, *Atmos. Chem. Phys.*, 2016, **16**, 1761–1771.
24 S. Wang, Y. Zhao, A. Chan, M. Yao, Z. Chen and J. Abbatt, *Chem. Rev.*, 2023, **123**, 1635–1679.
25 S. Paulson, P. Gallimore, X. Kuang, J. Chen, M. Kalberer and D. Gonzalez, *Sci. Adv.*, 2019, **5**, 5.
26 F. Li, S. Tang, J. Lv, S. Yu, X. Sun, D. Cao, Y. Wang and G. Jiang, *EGUsphere*, 2024, DOI: **10.5194/egusphere-2024-37**, preprint.
27 J. Wei, T. Fang and M. Shiraiwa, *ACS Environ. Au*, 2022, **2**, 336–345.
28 V. Lannuque, M. Camredon, F. Couvidat, A. Hodzic, R. Valorso, S. Madronich, B. Bessagnet and B. Aumont, *Atmos. Chem. Phys.*, 2018, **18**, 13411–13428.
29 Z. Wang, F. Couvidat and K. Sartelet, *Sci. Total Environ.*, 2024, **927**, 172142.
30 Y. Jo, M. Jang, S. Han, A. Madhu, B. Koo, Y. Jia, Z. Yu, S. Kim and J. Park, *Atmos. Chem. Phys.*, 2024, **24**, 487–508.
31 G. Cao and M. Jang, *Environ. Sci. Technol.*, 2010, **44**, 727–733.
32 Z. Wang, F. Couvidat and K. Sartelet, *Geosci. Model Dev.*, 2022, **15**, 8957–8982.
33 Z. Wang, F. Couvidat and K. Sartelet, *J. Aerosol Sci.*, 2023, **174**, 106248.
34 M. Jang and R. Kamens, *Environ. Sci. Technol.*, 2001, **35**, 3626–3639.
35 S. Wang, R. Wu, T. Berndt, M. Ehn and L. Wang, *Environ. Sci. Technol.*, 2017, **51**, 8442–8449.
36 Y. Li, J. Zhao, Y. Wang, J. Seinfeld and R. Zhang, *Environ. Sci. Technol.*, 2021, **55**, 8592–8603.

37 Z. Fu, F. Ma, Y. Liu, C. Yan, D. Huang, J. Chen, J. Elm, Y. Li, A. Ding, L. Pichelstorfer, H.-B. Xie, W. Nie, J. S. Francisco and P. Zhou, *Chem. Sci.*, 2023, **14**, 13050–13059.
38 D. Srivastava, W. Li, S. Tong, Z. Shi and R. M. Harrison, *Chemosphere*, 2023, **334**, 139002.
39 V. Lannuque, B. D'Anna, E. Kostenidou, F. Couvidat, A. Martinez-Valiente, P. Eichler, A. Wisthaler, M. Müller, B. Temime-Roussel, R. Valorso and K. Sartelet, *Atmos. Chem. Phys.*, 2023, **23**, 15537–15560.
40 S. Iyer, A. Kumar, A. Savolainen, S. Barua, C. Daub, L. Pichelstorfer, P. Roldin, O. Garmash, P. Seal, T. Kurtén and M. Rissanen, *Nat. Commun.*, 2023, **14**, 4984.
41 R. Schwantes, K. Schilling, R. Mcvay, H. Lignell, M. Coggon, X. Zhang, P. Wennberg and J. Seinfeld, *Atmos. Chem. Phys.*, 2017, **17**, 3453–3474.
42 K. Sartelet, F. Couvidat, Z. Wang, C. Flageul and Y. Kim, *Atmosphere*, 2020, **11**, 525.
43 K. Sartelet, F. Couvidat, C. Seigneur and Y. Roustan, *Atmos. Environ.*, 2012, **53**, 131–141.
44 Y. Kim, L. Lugon, A. Maison, T. Sarica, Y. Roustan, M. Valari, Y. Zhang, M. André and K. Sartelet, *Geosci. Model Dev.*, 2022, **15**, 7371–7396.
45 M. E. Jenkin, R. Valorso, B. Aumont, A. R. Rickard and T. J. Wallington, *Atmos. Chem. Phys.*, 2018, **18**, 9329–9349.
46 I. Suh, D. Zhang, R. Zhang, L. T. Molina and M. J. Molina, *Chem. Phys. Lett.*, 2002, **364**, 454–462.
47 R. Wu, S. Pan, Y. Li and L. Wang, *Atmos. Chem. Phys.*, 2014, **118**, 4533–4547.
48 D. Topping, M. Barley, M. K. Bane, N. Higham, B. Aumont, N. Dingle and G. McFiggans, *Geosci. Model Dev.*, 2016, **9**, 899–914.
49 P. B. Myrdal and S. H. Yalkowsky, *Ind. Eng. Chem. Res.*, 1997, **36**, 2494–2499.
50 Y. Nannoolal, J. Rarey, D. Ramjugernath and W. Cordes, *Fluid Phase Equilib.*, 2004, **226**, 45–63.
51 M. E. Jenkin, S. M. Saunders, V. Wagner and M. J. Pilling, *Atmos. Chem. Phys.*, 2003, **3**, 181–193.
52 C. Bloss, V. Wagner, M. E. Jenkin, R. Volkamer, W. J. Bloss, J. D. Lee, D. E. Heard, M.-R. M. Wirtz, G. Rea, J. C. Wenger and M. J. Pilling, *Atmos. Chem. Phys.*, 2005, **5**, 641–664.
53 J. Hu, Z. Chen, X. Qin and P. Dong, *Atmos. Chem. Phys.*, 2022, **22**, 6971–6987.
54 F. Couvidat, E. Debry, K. Sartelet and C. Seigneur, *J. Geophys. Res.*, 2012, **117**, year.
55 L. Lugon, K. Sartelet, Y. Kim, J. Vigneron and O. Chrétien, *Faraday Discuss.*, 2021, **226**, 432–456.
56 A. Maison, C. Flageul, B. Carissimo, A. Tuzet and K. Sartelet, *Atmosphere*, 2022, **13**, 527.
57 R. Macdonald, R. Griffiths and D. Hall, *Atmos. Environ.*, 1998, **32**, 1857–1864.
58 Z. Wang, F. Couvidat and K. Sartelet, *Geosci. Model Dev.*, 2022, **15**, 8957–8982.
59 Q. Huang, L. Wang and S. Han, *Chemosphere*, 1995, **30**, 915–923.